J Math Imaging Vis (2015) 52:345–355
DOI 10.1007/s10851-015-0568-x

Retinex by Higher Order Total Variation L^1 Decomposition

Jingwei Liang · Xiaoqun Zhang

Received: 30 June 2014 / Accepted: 3 February 2015 / Published online: 10 March 2015

Abstract In this paper, we propose a reflectance and illumination decomposition model for the Retinex problem via high-order total variation and L^1 decomposition. Based on the observation that illumination varies smoother than reflectance, we propose a convex variational model which can effectively decompose the gradient field of images into salient edges and relatively smoother illumination field through the first- and second-order total variation regularizations. The proposed model can be efficiently solved by a primal–dual splitting method. Numerical experiments on both grayscale and color images show the strength of the proposed model with applications to Retinex illusions, medical image bias field removal, and color image shadow correction.

Keywords Retinex · Image decomposition · High-order total variation · Shadow correction

1 Introduction

In the past decades, the study of the Retinex problem has inspired a wide range of applications and discussions [3,14,21]. The Retinex theory is originally proposed by Land and McCann [14] as a model of color perception of the human visual system (HVS), whose idea is that HVS can ascertain reflectance of a field in which both illumination and reflectance are unknown. Our visual system tends to see the same color of a given scene regardless of different illumination conditions. In other words, it ensures that the color of the objects remains relatively constant under varying illuminations. One of the most well-known Retinex illusions is the Adelson's checkerboard shadow illusion[1] shown in Fig. 1. Visually, region A of Fig. 1a seems darker than region B, while digitally these two regions have exactly the same intensity value. This phenomena is caused by different illumination conditions, and the perceived intensity of the objects is the combination of reflectance and illumination. By taking into account the surroundings of the object (shadow of the cylinder, periodic pattern of the checkerboard), our HVS discounts the illumination and perceive the reflectance automatically.

The primary goal of Retinex theory is to decompose a given image I into two components, reflectance R and illumination L such that

$$I(x) = R(x) \times L(x), \tag{1}$$

for $x \in \Omega$ where $\Omega \subset \mathbb{R}^2$ is the domain of the image. To simplify (1), one can apply the logarithm assuming that both R and L are positive which leads to

$$i(x) = r(x) + l(x). \tag{2}$$

Most of the decomposition methods are based on this additive model. The first Retinex algorithm proposed in [14] is based on path following, and further studied in [3,20]. Later

J. Liang
GREYC, CNRS UMR 6072, ENSICAEN, Université de Caen, Caen, France
e-mail: jingwei.liang@ensicaen.fr

X. Zhang (✉)
Department of Mathematics, MOE-LSC, and Institute of Natural Sciences, Shanghai Jiao Tong University, Shanghai, China
e-mail: xqzhang@sjtu.edu.cn

[1] http://web.mit.edu/persci/people/adelson/checkershadow_illusion.html

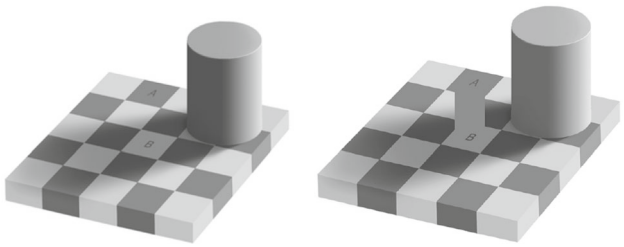

(a) original image **(b)** illusion free

Fig. 1 Checkerboard shadow illusion. **a** original checkerboard image, **b** illustration of illusion free image

on, the idea of path following is formulated into variational and PDE-based models. In [21], Morel et al. show that if the light paths are assumed to be symmetric random walks, then the Retinex solution satisfies a discrete Poisson equation and can be efficiently solved by using only two FFTs. Under variational framework, the followed total variation (TV) model [19] aims to extract piecewise constant reflectance r with data term in gradient field

$$\hat{r} = \arg\min_r \int_\Omega \Big(t|\nabla r| + \frac{1}{2}|\nabla r - \nabla i|^2\Big)\mathrm{d}x, \tag{3}$$

where $t > 0$ is the weight parameter. A simpler L^1-based model is proposed in [18], which reads

$$\hat{r} = \arg\min_r \int_\Omega |\nabla r - \delta_t(\nabla i)|\mathrm{d}x, \tag{4}$$

where $\delta_t(\nabla i)$ is the thresholded gradient field with respect to parameter t. This model appears to be efficient on suppressing the lighting effect of testing images, however, the loss of reflectance details and contrast can also be observed due to penalization on the magnitude of image gradient. Moreover, a rigorous analysis of the proposed model is missing. Recently, Zosso et al. [30] extended the TV-based models to a unified non-local formulation.

Decomposition models by penalizing both r and l simultaneously are also studied. For instance Kimmel et al. in [13] propose the followed TV + H^1 decomposition model

$$\hat{r} = \arg\min_r \int_\Omega \big(|\nabla r| + \alpha(r-i)^2 + \beta|\nabla(r-i)|^2\big)\mathrm{d}x, \tag{5}$$

where illumination $l = i - r$ is implicitly assumed to be smooth and penalized with H^1 norm. A similar model is further investigated by Ng and Wang in [22] with more constraints enforced. More specifically, the following minimization problem over both r and l is considered

$$\min_{r\le 0, l\ge i} \int_\Omega \Big(|\nabla r| + \frac{\alpha}{2}|\nabla l|^2 + \frac{\beta}{2}(i-r-l)^2 + \frac{\mu}{2}l^2\Big)\mathrm{d}x, \tag{6}$$

where the $l \ge i$ constraint is based on the assumption that $0 < R \le 1$.

In this paper, we also consider a decomposition approach to recover both r and l simultaneously. In particular, we focus on extracting illumination l using high-order regularization. Our proposed model is closely related to recently developed high-order total variation regularization. Therefore, in the following, we present some related models and notations.

1.1 High-Order Total Variation Methods

It is well known that total variation regularization [24] suffers the so-called staircase artifact. In order to suppress this effect, many higher order functionals have been studied since the pioneering infimal convolution model proposed in [5] on combining the first- and second-order total variation, which is defined as,

$$\big(\phi\triangle\psi\big)(u) = \inf_{u=v+w} \phi(v) + \psi(w),$$

where ϕ and ψ are two functionals.

The infimal convolution of the first- and second-order variations proposed in [5] with weight takes the form

$$J_\beta(u) = \inf_{v+w=u} \int_\Omega |\nabla v|\mathrm{d}x + \beta\int_\Omega |\nabla^2 w|\mathrm{d}x, \tag{7}$$

where $\int_\Omega |\nabla^2 w|$ denotes the total variation of the Hessian of w for $w \in W^{2,1}(\Omega)$. Thus, image u can now contain both piecewise constant and piecewise linear components. This formulation is restudied in [25,26] in the discrete setting for image restoration.

In a more general dual formulation, the infimal convolution of the first- and second-order total variation is defined as

$$\mathrm{ICTV}_\beta(u) = \sup_{\substack{p\in I_1\\ q\in I_2}} \inf_w \int_\Omega \big((u-w)\mathrm{div}(p) + \beta w\mathrm{div}^2(q)\big)\mathrm{d}x, \tag{8}$$

where $I_1 = \{p \in C_c^1(\Omega;\mathbb{R}^2), \|p\|_\infty \le 1\}$ and $I_2 = \{p \in C_c^2(\Omega;\mathbb{R}^{2\times 2}), \|p\|_\infty \le 1\}$. Note that if the symmetric Hessian is considered, we can also define $I_2 = \{p \in C_c^2\big(\Omega;\mathrm{Sym}^2(\mathbb{R}^2)\big), \|p\|_\infty \le 1\}$ where $\mathrm{Sym}^2(\mathbb{R}^2)$ denotes the space of symmetric matrices. Here, we abuse the notation of the infinity norm $\|\cdot\|_\infty$ in $C_c^1(\Omega;\mathbb{R}^2)$ and $C_c^2\big(\Omega;\mathrm{Sym}^2(\mathbb{R}^2)\big)$. A similar, yet different formulation, known as total generalized variation (TGV), is proposed and rigorously studied in [4]. In particular, the second-order TGV is defined as,

$$\mathrm{TGV}^2_\beta(u) = \sup_v \left\{ \int_\Omega u \mathrm{div}^2 v \mathrm{d}x \mid v \in \mathcal{C}^2_c\left(\Omega, \mathrm{Sym}^2\left(\mathbb{R}^2\right)\right), \right.$$
$$\left. \|v\|_\infty \le \beta,\ \|\mathrm{div} v\|_\infty \le 1 \right\}. \tag{9}$$

In a simplified form, the alternative primal form of (9) can be written as

$$\mathrm{TGV}^2_\beta(u) = \inf_{\boldsymbol{w}} \left\{ \int_\Omega |\nabla u - \boldsymbol{w}| \mathrm{d}x + \beta \int_\Omega |\nabla \boldsymbol{w}| \mathrm{d}x \right\}, \tag{10}$$

where $\nabla \boldsymbol{w} \in \mathbb{R}^{2\times 2}$ is the (symmetrized) gradient of the deformation field $\boldsymbol{w} \in \mathbb{R}^2$. This formulation can be also viewed as replacing the decomposition $u = v + w$ in (7) with the decomposition of the gradient field $\nabla u = \nabla v + \boldsymbol{w}$. More discussions on theoretical properties of the connections between the two functionals can be found in [1,4].

Another way of using high-order TV is the direct combination, not infimal convolution, of the first-order and higher order regularizations, such as [2,16,17,23]. For example [23] proposes a regularization model with direct combination of the first- and second-order TV for image restoration

$$\min_u \left\{ \frac{1}{2} \int_\Omega (Tu - u_0)^2 \mathrm{d}x \right.$$
$$\left. + \alpha \int_\Omega |\nabla u| \mathrm{d}x + \beta \int_\Omega |D^2 u| \mathrm{d}x \right\},$$

where T is a bounded linear operator and D is the gradient in distribute sense. This model has been studied in a more general and theoretical setting under the space of bounded Hessian. Finally, nonlinear high-order regularization [8,27], combining with curvature line (e.g. Euler's elastic), is also very popular, especially for image inpainting. In this paper, we focus more on the first- and second-order total variation.

1.2 Our Contributions

The infimal convolution of the first- and second-order total variation (in both ICTV and TGV) is designed to balance the first and high-order singularities presented in images. By involving higher order derivatives, these functionals can capture higher order edges instead of only piecewise constant components. It has been shown that these methods can suppress staircase artifact significantly.

From another point of view, formulation (10) [and (7)] decomposes ∇u field into two parts, L^1 norm of the residual $\nabla u - \boldsymbol{w}$ and TV semi-norm of $\boldsymbol{w}$. It is well known that TV + L^1 decomposition has interesting geometrical properties. As studied in [7,28], TV + L^1 decomposition model allows a scale-dependent decomposition of geometry features, which is invariant to image contrast. In Retinex theory, as considered in previous path following based work, the illumination varies relatively slower, hence can be considered having bigger scale in the gradient field. Furthermore, the nature of illumination often follows certain paths, thus piecewise linear approximation can model this behavior appropriately.

This motivates us to consider a decomposition model separating the higher order piecewise smooth components from the edges of relatively smaller scale in the gradient field. In particular, we propose to decompose the image i into the illumination l and reflectance r, and set the regularizations as

$$J(r) = \int_\Omega |\nabla r| \mathrm{d}x,$$
$$J_\beta(l) = \beta \int_\Omega |\nabla^2 l| \mathrm{d}x \tag{11}$$

We call this proposed approach higher order total variation L^1 (HoTVL1) illumination and reflectance decomposition model. Close connections to the previous infimal convolution models (7) and (10) are discussed, where we aim to extract higher order singularities as the smoother illumination component. To the best of our knowledge, this is also the first time that higher order infimal convolution model is used for the purpose of image decomposition. Furthermore, this model is different from the TV + H^1 decomposition model considered in [13,22], where the H^1 norm is penalized for illumination. In the section of numerical experiments, we show that the proposed model can better separate different scales of smoothness and singularities by TV + L^1 decomposition of the gradient field. Moreover compared to the L^1-based model [18], the proposed method can preserve better the edges with small magnitude without smearing out features of image with low intensities.

The rest of the paper is organized as following. In Sect. 2, we present the proposed model with constraints and discuss the connections with previous higher order regularization models. Furthermore, the existence and uniqueness of the solution for the proposed method are rigorously discussed in an extended functional space, i.e. , the product space of the bounded variation and bounded Hessian. In Sect. 3, a split inexact Uzawa based primal–dual splitting algorithm [29] is applied to solve the proposed model. Finally, we present numerical experiments on synthetic gray scale images, visual illusion images, medical images with bias filed and real color image examples, and compare the performance with some of the aforementioned existing variational-based methods.

2 High-Order TV + L^1 Decomposition Model

2.1 Proposed Model

Here, we present the first higher order TV + L^1 variational model for reflectance and illumination decomposition, which reads

$$\min_{r,l}\Big\{\mathcal{E}_{\alpha,\beta}(r,l)=\frac{1}{2}\int_\Omega (i-r-l)^2\mathrm{d}x + \alpha\Big(\int_\Omega |\nabla r|\mathrm{d}x+\beta\int_\Omega |\nabla^2 l|\mathrm{d}x\Big)\Big\}, \tag{12}$$

where l denotes illumination and r the reflectance, $\alpha > 0$, $\beta > 0$ are regularization parameters.

Roughly speaking, we extract relatively smoother piecewise linear component as l, and texture part as r in gradient field for Retinex decomposition. The proposed model can be interpreted as infimal convolution, where the connections are as following,

– Let $u = r + l$, then (12) is equivalent to

$$\begin{aligned}&\min_{u,l}\Big\{\frac{1}{2}\int_\Omega (u-i)^2\mathrm{d}x + \alpha\int_\Omega \big(|\nabla(u-l)|+\beta|\nabla^2 l|\big)\mathrm{d}x\Big\},\\ &\Longleftrightarrow \min_u\Big\{\frac{1}{2}\int_\Omega (u-i)^2\mathrm{d}x+\alpha\mathrm{ICTV}_\beta(u)\Big\}.\end{aligned} \tag{13}$$

– If we further replace ∇l by $\boldsymbol{v}=\begin{bmatrix}v_1\\ v_2\end{bmatrix}$ in (12), then we obtain the following model

$$\begin{aligned}&\min_{u,\boldsymbol{v}}\Big\{\frac{1}{2}\int_\Omega (u-i)^2\mathrm{d}x + \alpha\int_\Omega \big(|\nabla u-\boldsymbol{v}|+\beta|\nabla \boldsymbol{v}|\big)\mathrm{d}x\Big\},\\ &\Longleftrightarrow \min_u\Big\{\frac{1}{2}\int_\Omega (u-i)^2\mathrm{d}x+\alpha\mathrm{TGV}^2_\beta(u)\Big\}.\end{aligned} \tag{14}$$

Note that for both infimal convolution models, l is not explicitly given, while it can be extracted from numerical schemes or solved via the Poisson equation $\nabla l = \boldsymbol{v}$ with boundary conditions.

Model (12) and the infimal convolution (13), (14) have some drawbacks if we are interested in the solutions of r and l. It is easy to see that any solution pair $(\hat{r}+c, \hat{l}-c)$ with c being a constant is still a solution, and this non-uniqueness may greatly affect the quality of the solution. Furthermore, to show the existence of solutions, coercivity of the energy is also needed for the theoretical proof.

Therefore, we consider an extended version of model (12), which imposes box constraints on both r and l components

$$\min_{r\in\mathcal{B}_r, l\in\mathcal{B}_l}\Big\{\mathcal{E}_{\alpha,\beta,\tau}(r,l)=\frac{1}{2}\int_\Omega (i-r-l)^2\mathrm{d}x + \alpha\Big(\int_\Omega |\nabla r|\mathrm{d}x+\beta\int_\Omega |\nabla^2 l|\mathrm{d}x\Big)+\frac{\tau}{2}\int_\Omega l^2\mathrm{d}x\Big\}, \tag{15}$$

where τ is a small positive number to ensure the boundedness of l, $\mathcal{B}_r$ and $\mathcal{B}_l$ are the box constraints for r and l respectively. For instance, similar to the constraints considered in [22], one can consider $\mathcal{B}_r =]-\infty, 0]$ and $\mathcal{B}_l = [i, +\infty[$ under the assumptions that $R \in (0, 1]$.

2.2 Existence and Uniqueness of Solution

The functional $\mathcal{E}_{\alpha,\beta,\tau}(r,l)$ in (15) is defined on $W^{1,1}\times W^{2,1}$. To establish the existence for such regularization, we usually need to discuss a larger Banach space for r and l. More precisely, we consider r in the bounded variation space $\mathrm{BV}(\Omega)$ and l in the bounded Hessian space $\mathrm{BH}(\Omega)$, and show the existence of the solution pair (r, l) of the following functional in product space,

$$\min_{\substack{r\in\mathrm{BV}(\Omega)\\ l\in\mathrm{BH}(\Omega)}}\Big\{\mathcal{E}_{\alpha,\beta,\tau}(r,l)=\frac{1}{2}\|i-r-l\|^2 + \alpha\big(\|Dr\|_1+\beta\|D^2 l\|_1\big)+\frac{\tau}{2}\|l\|^2+\iota_{\mathcal{B}}(r,l)\Big\}, \tag{16}$$

where $\|\cdot\|$ denotes the norm in $L^2(\Omega)$, $\mathcal{B}$ denotes the box constraint

$$\mathcal{B}=\mathcal{B}_r\times\mathcal{B}_l,$$

$\iota_{\mathcal{B}}(\cdot)=\iota_{\mathcal{B}_r}(r)+\iota_{\mathcal{B}_l}(l)$ is the corresponding indicator function, $\|Dr\|_1$ and $\|D^2 l\|_1$ denote the total variation of the first- and second-order derivatives in distribution sense, which is defined later.

We first present some preliminaries for bounded Hessian space proposed in [9] and in [2,23] in the context of image restoration. Let Ω be an open subset of $\mathbb{R}^n$ with Lipschitz boundary, recall that the Sobolev space $W^{1,1}(\Omega)$ is defined as

$$W^{1,1}(\Omega)=\big\{u\in L^1(\Omega)\,|\,\nabla u\in L^1(\Omega)\big\}.$$

The standard total variation semi-norm in distribution sense is defined as

$$\|Du\|_1=\int_\Omega |Du|\mathrm{d}x=\sup_{\substack{p\in C_c^1(\Omega)^n\\ \|p\|_\infty\le 1}}\int_\Omega u\,\mathrm{div}\,p\,\mathrm{d}x, \tag{17}$$

where $\mathrm{div}\,p=\sum_{i=1}^n \frac{\partial p_i}{\partial x_i}(x)$.

Following Demengel [9] and [23], we consider the space of bounded Hessian functions $\mathrm{BH}(\Omega)$ (also called as $\mathrm{BV}^2(\Omega)$ in [2]) on extending the notion of total variation (17). Define

$$\begin{aligned}\|D^2u\|_1&=\int_\Omega |D^2u|\mathrm{d}x\\ &=\sup_{\substack{\xi\in C_c^2(\Omega;\mathbb{R}^{n\times n})\\ \|\xi\|_\infty\le 1}}\int_\Omega \langle\nabla u,\mathrm{div}(\xi)\rangle\mathrm{d}x,\end{aligned} \tag{18}$$

where $\mathrm{div}(\boldsymbol{\xi}) = (\mathrm{div}\xi_1, \cdots, \mathrm{div}\xi_n)$ with

$$\forall i, \xi_i = \left\{\xi_i^{(1)}, \cdots, \xi_i^{(n)}\right\} \in \mathbb{R}^n, \mathrm{div}\xi_i = \sum_{k=1}^{n} \frac{\partial \xi_i^{(k)}}{\partial x_k},$$

and $\|\xi\|_\infty = \sup_{x\in\Omega} \sqrt{\sum_{i,j=1}^{n} |\xi_i^{(j)}(x)|^2}$. The space $\mathrm{BH}(\Omega)$ consists of all functions $u \in W^{1,1}(\Omega)$ whose distributional Hessian is a finite Radon measure, i.e.

$$\mathrm{BH}(\Omega) = \left\{u \in W^{1,1}(\Omega) \,|\, \|D^2 u\|_1 < \infty\right\}.$$

It is immediate to see that $W^{2,1}(\Omega) \subset \mathrm{BH}(\Omega)$ and $\mathrm{BH}(\Omega)$ is a Banach space equipped with norm $\|u\|_{\mathrm{BH}(\Omega)} = \|u\|_1 + \|\nabla u\|_1 + \|D^2 u\|_1$, where $\|\cdot\|_1$ denotes the L^1 norm in the corresponding space. In the following, we summarize some definitions and main properties in $\mathrm{BH}(\Omega)$, which can be found in [2,9,23]:

– (A weak* topology) Let $\{u_k\}_{k\in\mathbb{N}}$, u belong to $\mathrm{BH}(\Omega)$. Sequence $\{u_k\}$ converges to u weakly* in $\mathrm{BH}(\Omega)$ if

$$\|u_k - u\|_1 \to 0, \|\nabla u_k - \nabla u\|_1 \to 0,$$
$$\int_\Omega \langle \nabla u_k, \mathrm{div}(\boldsymbol{\xi})\rangle \mathrm{d}x \longrightarrow \int_\Omega \langle \nabla u,\ \mathrm{div}(\boldsymbol{\xi})\rangle \mathrm{d}x, \forall \boldsymbol{\xi} \in C_c^2(\Omega; \mathbb{R}^{n\times n}). \quad (19)$$

– (Lower semi-continuity) The semi-norm $\|D^2 u\|_1$ is lower semi-continuous endowed with strong topology of $W^{1,1}(\Omega)$. More precisely, if $\|u_k - u\|_1 \to 0$ and $\|\nabla u_k - \nabla u\|_1 \to 0$, then

$$\|D^2 u\|_1 \le \liminf_{k\to\infty} \|D^2 u_k\|_1.$$

In particular, for $\{u_k\}_{k\in\mathbb{N}} \in W^{1,1}(\Omega)$, if

$$\liminf_{k\to\infty} \|D^2 u_k\|_1 < \infty,$$

then $u \in \mathrm{BH}(\Omega)$.

– (Compactness in $\mathrm{BH}(\Omega)$) Suppose that $\{u_k\}_{k\in\mathbb{N}}$ is bounded in $\mathrm{BH}(\Omega)$, then there exists a subsequence $\{u_{k_j}\}_{j\in\mathbb{N}}$ and $u \in \mathrm{BH}(\Omega)$ such that $\{u_{k_j}\}_{j\in\mathbb{N}}$ weakly* converges to u.

– (Embedding) If Ω has a Lipschitz boundary and it is connected, then it can be shown that there exists positive constants C_1, C_2 such that

$$\|\nabla u\|_1 \le C_1 \|D^2 u\|_1 + C_2 \|u\|_1, \quad (20)$$

and $\mathrm{BH}(\Omega)$ is continuously embedded in $L^2(\Omega)$ when $n = 2$.

In the following, we use the above-mentioned properties of $\mathrm{BH}(\Omega)$ together with similar ones of $\mathrm{BV}(\Omega)$ to establish the existence and uniqueness of solution for problem (16).

Theorem 1 *Suppose $i \in L^2(\Omega)$ and $\alpha, \beta, \tau > 0$, then problem (16) admits a unique solution pair $(r^*, l^*) \in \mathrm{BV}(\Omega) \times \mathrm{BH}(\Omega)$.*

Proof Let $\{(r_k, l_k)\}_{k\in\mathbb{N}}$ be a minimizing sequence of (16), and $M > 0$ be the upper bound of the sequence such that

$$\|r_k + l_k - i\|^2 < M, \quad \|l_k\|^2 < M, \quad (21)$$
$$\|Dr_k\|_1 < M, \quad \|D^2 l_k\|_1 < M, \quad (22)$$
$$r_k \in \mathcal{B}_r, \quad l_k \in \mathcal{B}_l, \quad (23)$$

for every $k \in \mathbb{N}$. Since $\{l_k\}_{k\in\mathbb{N}}$ is uniformly bounded in $L^2(\Omega)$, it is easy to see that $\{r_k\}_{k\in\mathbb{N}}$ is also uniformly bounded in $L^2(\Omega)$ combining with (21) and $i \in L^2(\Omega)$. Moreover, by the boundedness of Ω, sequence $\{r_k\}$ is bounded in $L^1(\Omega)$ and moreover bounded in $\mathrm{BV}(\Omega)$ since $\|Dr_k\|_1 < M$.

For $\{l_k\}$, we can derive similarly that $\{l_k\}$ is bounded in $L^1(\Omega)$. By virtue of the embedding inequality (20), we also have

$$\|\nabla l_k\|_1 < C_1 \|D^2 l_k\|_1 + C_2 \|l_k\|_1 < M',$$

where M' is a constant number for all $k \in \mathbb{N}$. Thus $\{l_k\}$ is uniformly bounded in $\mathrm{BH}(\Omega)$.

From the compactness theorem in both BV and BH spaces, we can obtain a subsequence (r_{k_j}, l_{k_j}) converging weakly* to (r^*, l^*) in $\mathrm{BV}(\Omega) \times \mathrm{BH}(\Omega)$. It is easy to see that the functional is proper since any constant function l and r has finite energy. Furthermore, the overall functional $\mathcal{E}_{\alpha,\beta,\tau}$ is convex and l.s.c under weak topology, the constraint sets $\mathcal{B}_r$ and $\mathcal{B}_l$ are closed, therefore we can derive that the minima can be attained at (r^*, l^*) by the theory of calculus of variation. It is also straightforward to see that the solution is unique since the functional is strongly convex with respect to (r, l). □

3 Primal–Dual Splitting Algorithm

In this section, we present the algorithm for solving the discrete version of (15), which has been well studied in the literature. For instance the widely used split Bregman method [12] and primal–dual splitting methods [6,10] based on operator splitting techniques. Here, we adopt the split inexact Uzawa (SIU) method developed in [29] which yields a simple iteration scheme for our problem.

Note also that the two unknowns r, l are coupled in (15), therefore, an inner alternating scheme is applied in order to fully decouple the sub-problems for r and l. However, it should be mentioned that such alternating scheme does not guarantee the whole sequence converge to the minimizer of the original problem.

We first define some variables and notations to simplify (15). Denote

$$x = \begin{bmatrix} r \\ l \end{bmatrix}, \quad A = \begin{bmatrix} \mathrm{Id}, & \mathrm{Id} \end{bmatrix}, \quad B = \begin{bmatrix} 0, & \mathrm{Id} \end{bmatrix},$$

and the auxiliary ones

$$u = \nabla r, \quad v = \nabla^2 l,$$
$$y = \begin{bmatrix} u \\ v \end{bmatrix}, \quad \text{and} \quad L = \begin{bmatrix} \nabla, & 0 \\ 0, & \nabla^2 \end{bmatrix}.$$

Here, we use forward difference and Neumann boundary conditions for the discrete gradient and symmetrized Hessian. In $\mathbb{R}^2$, for $u \in W^{1,1}(\Omega)$, define

$$D(\nabla u) = \frac{1}{2}\left(D + D^T\right)(\nabla u) = \begin{bmatrix} \xi_{11}, & \xi_{12} \\ \xi_{21}, & \xi_{22} \end{bmatrix},$$

as the symmetrized Hessian, where

$$\begin{aligned} &\xi_{11} = \frac{\partial v_1}{\partial x_1}, \ \xi_{22} = \frac{\partial v_2}{\partial x_2}, \\ &\xi_{12} = \xi_{21} = \frac{1}{2}\left(\frac{\partial v_1}{\partial x_2} + \frac{\partial v_2}{\partial x_1}\right), \end{aligned} \tag{24}$$

for $\boldsymbol{v} = \begin{bmatrix} v_1 \\ v_2 \end{bmatrix} = \nabla u$ and the divergence can be defined accordingly.

We further define the following functionals,

$$H(x) = \frac{1}{2}\|i - Ax\|^2,$$
$$J(x, y) = \alpha\|y\|_{1,\beta} + \iota_{\mathcal{B}}(x) + \frac{\tau}{2}\|Bx\|^2,$$

where $\|y\|_{1,\beta} = \|u\|_1 + \beta\|v\|_1$. As a result, (15) can be formulated into the following form

$$\min_{x,y} H(x) + J(x, y) \text{ s.t. } Lx = y, \tag{25}$$

whose augmented Lagrangian formula is

$$\begin{aligned} \max_{p} \min_{x,y} \Big\{ &\mathcal{L}(p; x, y) = H(x) + J(x, y) \\ &+ \langle p, Lx - y\rangle + \frac{\nu}{2}\|Lx - y\|^2 \Big\}, \end{aligned} \tag{26}$$

where $p = \begin{bmatrix} p_r \\ p_l \end{bmatrix}$ is the Lagrangian multiplier.

The SIU method is an inexact variant of alternating direction method of multipliers (ADMM) [11] applied to the above problem with an extra proximal term for the update of x^{k+1}, which reads

$$\begin{cases} x^{k+1} = \arg\min_x \mathcal{L}\left(p^k; x, y^k\right) + \frac{1}{2}\|x - x^k\|_{M_\nu}, \\ y^{k+1} = \arg\min_y \mathcal{L}\left(p^k; x^{k+1}, y\right), \\ p^{k+1} = p^k + \nu\left(Lx^{k+1} - y^{k+1}\right), \end{cases} \tag{27}$$

where M_ν is a positive definite matrix. To obtain an easy iterative scheme, we choose $M_\nu = \mathrm{Id} - \nu L^{TL}$, where $0 < \nu < 1/\|L^{TL}\|$.

In the following, we present a brief derivation for the update of x^{k+1} and y^{k+1} respectively.

Update of x^{k+1}: Let $M_\nu = \mathrm{Id} - \nu L^{TL}$, then

$$\begin{aligned} x^{k+1} &= \arg\min_x \mathcal{L}\left(p^k; x, y^k\right) + \frac{1}{2}\|x - x^k\|^2_{M_\nu} \\ &= \arg\min_x \iota_{\mathcal{B}}(x) + \frac{1}{2}\|i - Ax\|^2 \\ &\quad + \frac{\tau}{2}\|Bx\|^2 + \frac{1}{2}\|x - w^k\|^2, \end{aligned} \tag{28}$$

where $w^k = x^k - L^T(\nu L x^k + p^k - \nu y^k) = \begin{bmatrix} w_r^k \\ w_l^k \end{bmatrix}$. The corresponding first order optimality condition of (28) is

$$\begin{aligned} 0 &\in N_{\mathcal{B}}(x) + A^T(Ax - i) + \tau B^T Bx + (x - w^k) \\ &\in \begin{bmatrix} N_{\mathcal{B}_r}(r) \\ N_{\mathcal{B}_l}(l) \end{bmatrix} + \begin{bmatrix} r + l - i \\ r + l - i \end{bmatrix} + \tau \begin{bmatrix} 0 \\ l \end{bmatrix} + \begin{bmatrix} r - w_r^k \\ l - w_l^k \end{bmatrix}. \end{aligned}$$

Let $\tilde{w}_r = w_r^k + i$, $\tilde{w}_l = w_l^k + i$, and $\mathcal{P}_{\mathcal{C}}$ the projection operator onto a nonempty closed convex set $\mathcal{C}$. In the following, we discuss the updating formula under different scenarios of the box constraints $\mathcal{B}$.

– If $\mathcal{B}_l = \mathbb{R}$, which implies that there is no constraint on l, we have

$$\begin{cases} N_{\mathcal{B}_r}(r) + 2r + l = \tilde{w}_r, \\ r + (\tau + 2)l = \tilde{w}_l. \end{cases}$$

Substituting the second equation in the first one, we obtain

$$N_{\mathcal{B}_r}(r) + \frac{2\tau + 3}{\tau + 2}r = \tilde{w}_r - \frac{\tilde{w}_l}{\tau + 2}.$$

Thus, the update formula for r^{k+1} and l^{k+1} reads

$$\begin{cases} r^{k+1} = \mathcal{P}_{\mathcal{B}_r}\left(\dfrac{(\tau + 2)\tilde{w}_r - \tilde{w}_l}{2\tau + 3}\right), \\ l^{k+1} = \dfrac{\tilde{w}_l - r^{k+1}}{\tau + 2}. \end{cases}$$

– If $\mathcal{B}_r = \mathbb{R}$, similarly we get

$$\begin{cases} 2r + l = \tilde{w}_r, \\ 2N_{\mathcal{B}_l}(l) + (2\tau + 3)l = 2\tilde{w}_l - \tilde{w}_r. \end{cases}$$

And the update formula for r^{k+1} and l^{k+1} are

$$\begin{cases} l^{k+1} = \mathcal{P}_{\mathcal{B}_l}\left(\dfrac{2\tilde{w}_l - \tilde{w}_r}{2\tau + 3}\right), \\ r^{k+1} = \dfrac{\tilde{w}_r - l^{k+1}}{2}. \end{cases}$$

– If both $\mathcal{B}_r$ and $\mathcal{B}_l$ are not the whole space, then the subproblem is coupled on r and l, and an alternating projection method is applied, which reads

$$\begin{cases} r \leftarrow \mathcal{P}_{\mathcal{B}_r}\left(\dfrac{\tilde{w}_r - l}{2}\right), \\ l \leftarrow \mathcal{P}_{\mathcal{B}_l}\left(\dfrac{\tilde{w}_l - r}{2 + \tau}\right). \end{cases} \tag{29}$$

Note that in theory many iterations are needed for this step to get accurate r^{k+1}, l^{k+1}.

Update of y^{k+1}: The update of y^{k+1} is rather simple. As $\|y\|_{1,\beta} = \|u\|_1 + \beta\|v\|_1$ is separable, we have

$$\begin{aligned} y^{k+1} &= \arg\min_y \mathcal{L}(p^k; x^{k+1}, y) \\ &= \arg\min_y \alpha\|y\|_{1,\beta} + \frac{\nu}{2}\|y - Lx^{k+1} - p^k/\nu\|^2 \\ &= \arg\min_{u,v} \alpha\|u\|_1 + \frac{\nu}{2}\|u - \nabla r^{k+1} - p_r^k/\nu\|^2 \\ &\quad + \alpha\beta\|v\|_1 + \frac{\nu}{2}\|v - \nabla^2 l^{k+1} - p_l^k/\nu\|^2, \end{aligned}$$

which leads to the following two simple threshold steps

$$\begin{cases} u^{k+1} = \mathcal{T}_{\alpha/\nu}\left(\nabla r^{k+1} + p_r^{k+1}/\tau\right), \\ v^{k+1} = \mathcal{T}_{\alpha\beta/\nu}\left(\nabla^2 l^{k+1} + p_l^{k+1}/\tau\right), \end{cases} \tag{30}$$

where $\mathcal{T}_\gamma(a) = \max(\|a\| - \gamma, 0)\frac{a}{\|a\|}$ is the isotropic soft-threshold operator.

Finally, the update for the dual variable p^{k+1} is straightforward. To this end, combining (29), (30) and the update of p^{k+1} (27) we obtain the iteration scheme for solving (15).

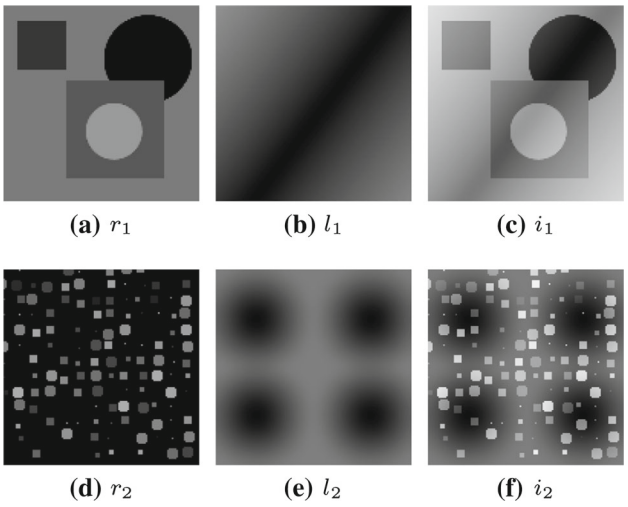

(a) r_1 **(b)** l_1 **(c)** i_1 **(d)** r_2 **(e)** l_2 **(f)** i_2

Fig. 2 Two synthetic image examples. **a** synthetic image r_1, **b** synthetic shadow l_1, **c** composed image $i_1 = r_1 + l_1$; **d** synthetic image r_2, **e** synthetic shadow l_2, **f** composed image $i_2 = r_2 + l_2$

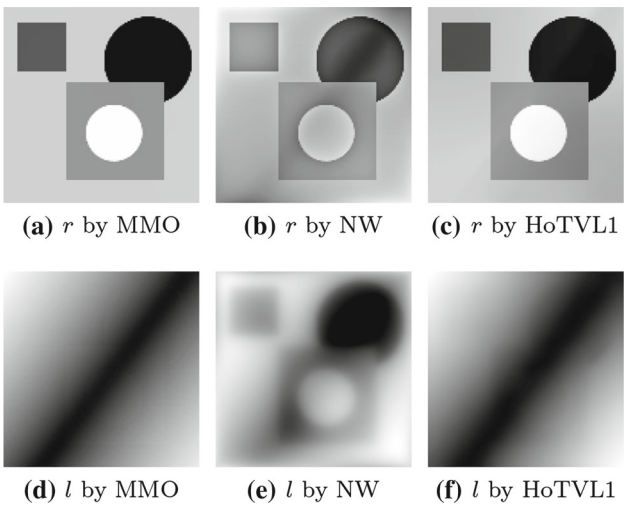

(a) r by MMO **(b)** r by NW **(c)** r by HoTVL1 **(d)** l by MMO **(e)** l by NW **(f)** l by HoTVL1

Fig. 3 Decomposition comparison of synthetic example 1. From *top* to *bottom* and from *left* to *right*: recovered reflectance r and illumination l by MMO, NW, and the proposed method

4 Numerical Tests

To demonstrate the performance of our proposed method, in this section, we consider several image decomposition problems, including synthetic examples, Retinex illusion examples, medical image bias field removal and color image shadow correction. We compare our proposed method (15) (HoTVL1) with two recent variational methods (4) (MMO) and (6) (NW) proposed in [18] and [22] respectively.

For all the tests, the recovered r of MMO and our method are the direct outputs from the model, so is NW method for the synthetic example and Retinex problem. While for the bias field removal and color image shadow correction, the output r of NW method is obtained via $i - l$.

4.1 Synthetic Images

We start with synthetic examples with two different cases. As shown in Fig. 2, two piecewise constant images r with different geometry properties, so are the corresponding shadows l with piecewise smooth structures, and the simulated image is the sum of them, namely $i = r + l$.

Decomposition results are shown in Figs. 3 and 4. As we can observe, MMO and HoTVL1 produce better visual

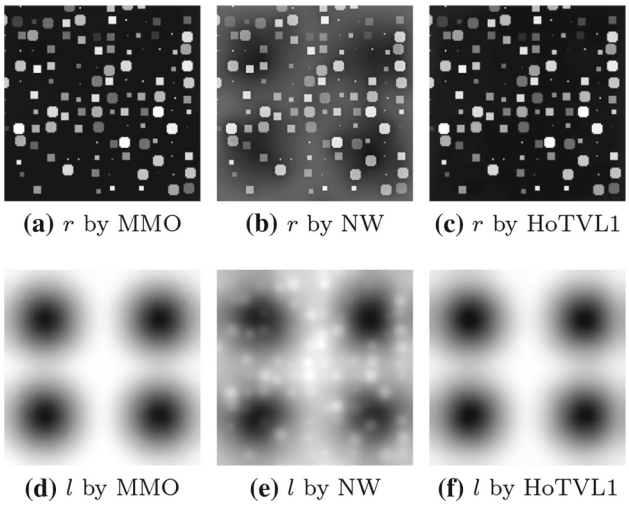

Fig. 4 Decomposition comparison of synthetic example 2. From *top* to *bottom* and from *left* to *right*: recovered reflectance r and illumination l by MMO, NW, and the proposed method

Table 1 Recovered intensity values of regions A and B of the two images

Image		Original	MMO	NW	HoTVL1
Checker-board	A	120	80	90	85
	B	120	145	125	174
Cube	A	140	26	85	10
	B	140	191	110	250

results than NW method on these examples. Intuitively, NW method penalizes the ℓ_2-norm of the gradient of the illumination which is not contrast invariant, hence the recovered illumination l contains more information of the edges of reflectance. On the contrast, only very weak signal of r is contained in the recovered illumination l by MMO method and our proposed method. This will be further demonstrated in Retinex illusion and color image examples.

For this example, we set $\beta = 10$ for both examples, $\alpha = 2$ for the first synthetic image, and $\alpha = 4$ for the second one. Both of the box constraints are $[0, 255]$.

4.2 Retinex Illusion

The aforementioned checkerboard shadow image and the Logvinenko's cube shadow illusion image [15], as shown in Fig. 5, are tested for Retinex illusion. For both images, though visually region B is brighter than region A, they are of the same intensity value.

Table 1 shows the comparison of the recovered intensity values of the two regions of the three methods. Our proposed method recovers the best contrast compared to the other two on both images.

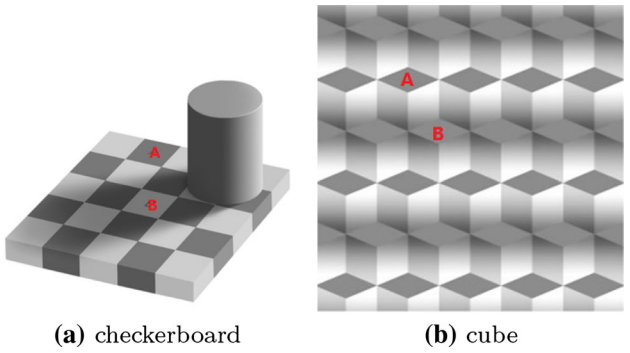

Fig. 5 Two test images for Retinex illusion. **a** Adelson's checkerboard shadow image, the intensity value of the marked area is 120. **b** Logvinenko's cube shadow image, the intensity value of the marked area is 140

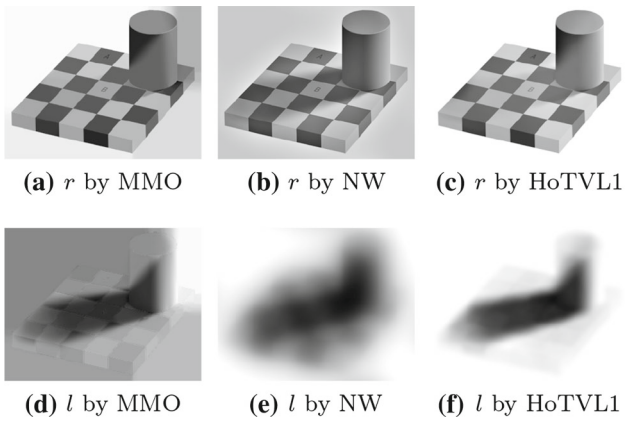

Fig. 6 Decomposition comparison of the checkerboard example. From *top* to *bottom* and from *left* to *right*: recovered reflectance r and illumination l by MMO, NW, and the proposed model

Figure 6 shows the visual comparison on the checkerboard image. Similar to the synthetic example, MMO and the proposed method obtain visually preferable outputs, however, the recovered illumination in our proposed method contains less reflectance information compared to MMO. Similar conclusions can be drawn from the comparison of the cube image, see Fig. 7.

It can be noticed that the brightness of MMO's result and ours is very different, especially for Fig. 7. This is mainly due to the fact that for MMO method, the intensity value of the top left pixel is used to solve the Poisson equation, also the right column and bottom row of the output is brighter than the other parts of the image due to boundary condition.

In this test, $\beta = 10$ for both examples, and we set $\alpha = 4$ for the checkerboard image, and $\alpha = 10$ the cube image. The box constraints are $\mathcal{B}_r = [0, 255]$ and $\mathcal{B}_l = [-255, 0]$ for both images.

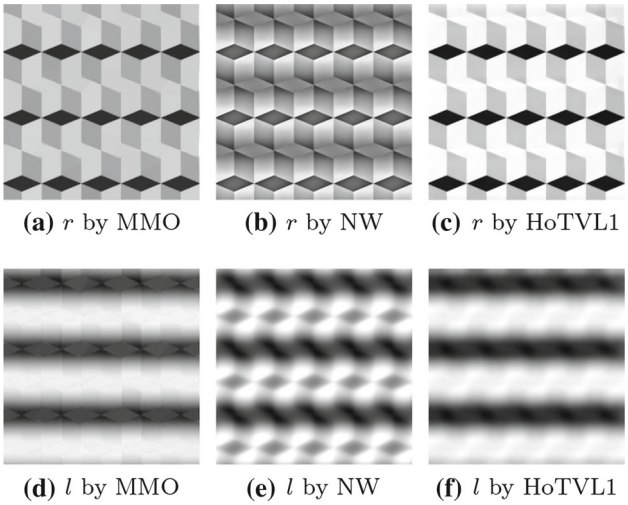

(a) r by MMO **(b)** r by NW **(c)** r by HoTVL1

(d) l by MMO **(e)** l by NW **(f)** l by HoTVL1

Fig. 7 Decomposition comparison of the cube example. From *top* to *bottom* and from *left* to *right*: recovered reflectance r and illumination l by MMO, NW, and the proposed method

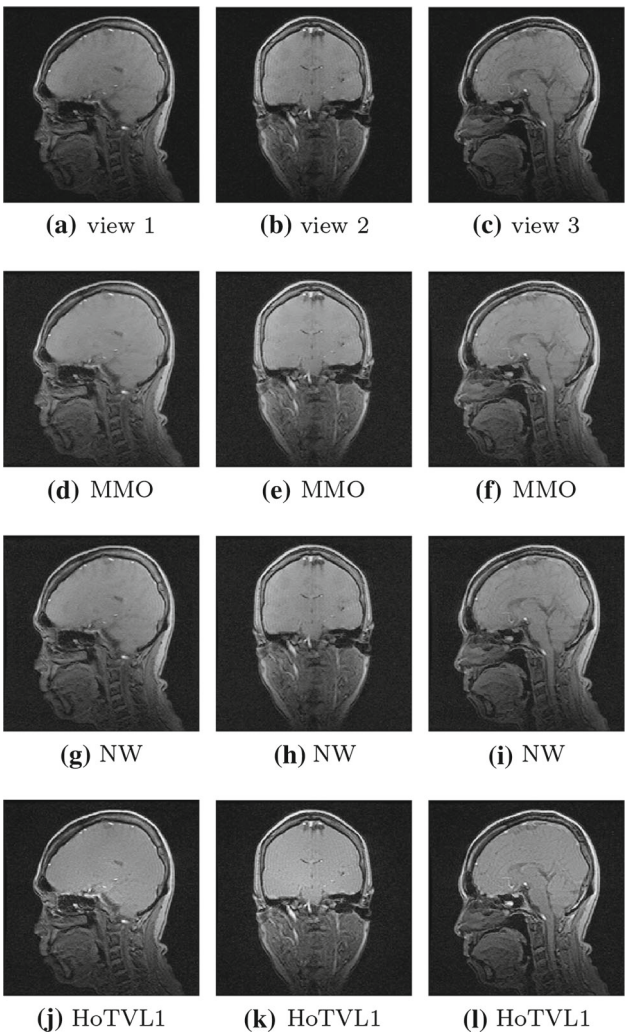

(a) view 1 **(b)** view 2 **(c)** view 3

(d) MMO **(e)** MMO **(f)** MMO

(g) NW **(h)** NW **(i)** NW

(j) HoTVL1 **(k)** HoTVL1 **(l)** HoTVL1

Fig. 8 MRI image bias field removal. **a**, **d**, **g**, **j** image view 1 and the result of the three methods; **b**, **e**, **h**, **k** image view 2 and the result of the three methods; **c**, **f**, **i**, **l** image view 3 and the result of the three methods

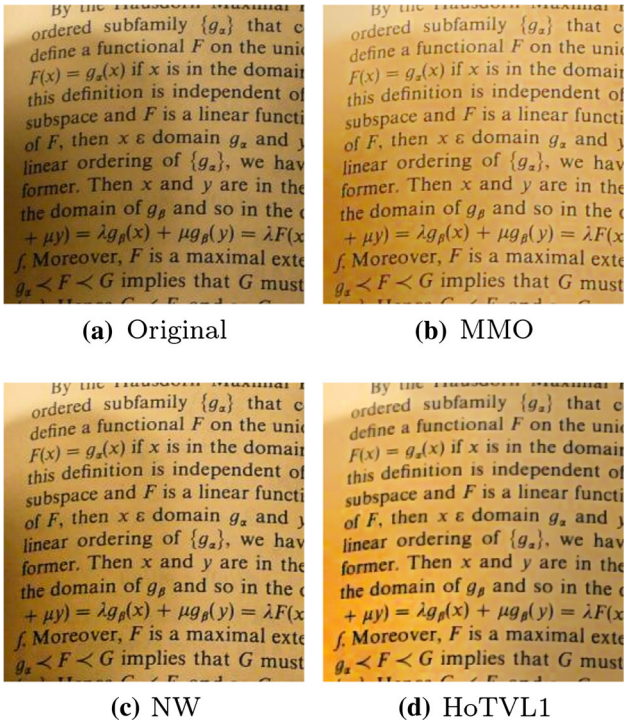

(a) Original **(b)** MMO

(c) NW **(d)** HoTVL1

Fig. 9 Comparison of recovered reflectance r on Text image

4.3 Medical image bias field correction

In medical imaging, the obtained images may be corrupted by bias fields due to non-uniform illuminations, parallel MRI imaging for example. The correction of the bias field is similar to Retinex problem where we need to remove the light effect caused by illumination. Here, we adopt the settings discussed in [18], and Fig. 8 shows the comparison of the methods. As observed, all methods can provide visual preferable results compared to the original ones, especially for the bottom part of the images.

For this example, we set $\alpha = 1/10$ and $\beta = 20$. The box constraints are $\mathcal{B}_r = [-20, 0]$ and $\mathcal{B}_l = [-20, 0]$ after taking the logarithm, and I is pre-scaled to $(0, 1]$.

4.4 Color Image Shadow Correction

The final illustrative example is the correction of shadowed color image. For the two color images given in Figs. 9a and 10a, we choose the HSV (hue, saturation, value) color space and only process the V channel, assuming that shadow affects only the brightness of the image. Figure 9 shows the comparison on the text image. Note that NW method also adopts one-step γ-correction as post-processing, which may improve the contrast of under-exposed images. We can see that the estimated shadow of our method is visually more accurate and the shadow effect can be partially removed in the recov-

(a) Original (b) MMO

(c) NW (d) HoTVL1

Fig. 10 Comparison of recovered reflectance r on Wall image

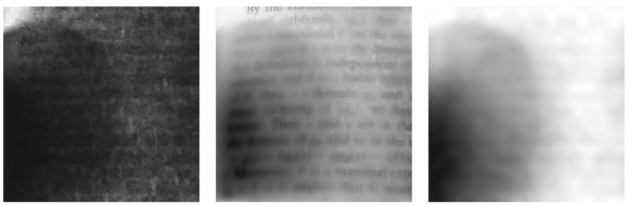

(a) MMO (b) NW (c) HoTVL1

Fig. 11 Comparison of recovered illumination l on Text image

(a) MMO (b) NW (c) HoTVL1

Fig. 12 Comparison of recovered illumination l on Wall image

ered reflectance. Similar observation can be obtained from Figs. 11 and 12.

For this test, we set $\alpha = 1/12$ for text image and $1/10$ for the wall image, $\beta = 10$ is fixed. The box constraints are the same as the bias field correction's.

4.5 Computational Time

To conclude this part, we present the computational time comparison of the three methods. Since we have box constraints for both r and l, inner iteration is needed for the update of x^{k+1}, and the number of iterations is set as 1 for all tests. Among the methods, MMO method is the fastest due to its simplicity, NW method is the second, and our proposed method is more time consuming mainly due to the second-order TV regularization. For example in the synthetic example with image size 128×128, it takes less than 1 s for the MMO method, around 1 s for the NW, while around 15 s for our method. However, the computational time of our method can be improved by choosing more efficient algorithms.

5 Conclusions

In this paper, we have presented a novel reflectance and illumination decomposition model based on high-order TV + L^1 regularization, which is closely related to the infimal convolution of first- and second-order TV regularizations. The proposed model can nicely separate the relatively smoother piecewise linear component, which is modeled as the global illumination, from the relatively detailed reflectance edges. Numerical experiments on inhomogeneous background removal and color shadow correction have shown that our proposed model extracts HVS preferable illumination, and detail preserved reflectance, comparing to other decomposition models [18,22].

Acknowledgments We would like to thank the authors of [18] and [22] for sharing their source codes, and the reviewers of this manuscript for their helpful comments and suggestions. The work of X. Zhang was supported by NSFC11101277, NSFC91330102 and 973 program (#2015CB856000).

References

1. Benning, M., Brune, C., Burger, M., Müller, J.: Higher-order TV methods-enhancement via Bregman iteration. J. Sci. Comput. **54**(2–3), 269–310 (2013). doi:10.1007/s10915-012-9650-3
2. Bergounioux, M., Piffet, L.: A second-order model for image denoising. Set. Valued Var. Anal. **18**(3–4), 277–306 (2010). doi:10.1007/s11228-010-0156-6
3. Bertalmo, M., Caselles, V., Provenzi, E.: Issues about Retinex theory and contrast enhancement. Int. J. Comput. Vis. **83**(1), 101–119 (2009). doi:10.1007/s11263-009-0221-5
4. Bredies, K., Kunisch, K., Pock, T.: Total generalized variation. SIAM J. Imaging Sci. **3**(3), 492–526 (2010). doi:10.1137/090769521
5. Chambolle, A., Lions, P.L.: Image recovery via total variation minimization and related problems. Numer. Math. **76**(2), 167–188 (1997). doi:10.1007/s002110050258
6. Chambolle, A., Pock, T.: A first-order primal-dual algorithm for convex problems with applications to imaging. J. Math. Imaging Vis. **40**(1), 120–145 (2011). doi:10.1007/s10851-010-0251-1

7. Chan, T.F., Esedolu, S.: Aspects of total variation regularized ℓ_1 function approximation. SIAM J. Appl. Math. **65**(5), 1817–1837 (2005). http://www.jstor.org/stable/4096154
8. Chan, T.F., Kang, S.H.: Euler's elastica and curvature based inpaintings. SIAM J. Appl. Math. **63**, 564–592 (2002). doi:10.1137/S0036139901390088
9. Demengel, F.: Fonctions hessien born. Annales de l'institut Fourier **34**(2), 155–190 (1984). http://eudml.org/doc/74627
10. Esser, E., Zhang, X., Chan, T.F.: A general framework for a class of first order primal-dual algorithms for convex optimization in imaging science. SIAM J. Imaging Sci. **3**, 1015–1046 (2010). doi:10.1007/s10915-010-9408-8
11. Gabay, D.: Applications of the method of multipliers to variational inequalities, Augmented Lagrangian methods: applications to the solution of boundary-value problems, **15**, chap. IX, pp. 299–331 (1983)
12. Goldstein, T., Osher, S.: The split Bregman method for ℓ_1-regularized problems. SIAM J. Imaging Sci. **2**(2), 323–343 (2009). doi:10.1137/080725891
13. Kimmel, R., Elad, M., Shaked, D., Keshet, R., Sobel, I.: A variational framework for Retinex. Int. J. Comput. Vis. **52**(1), 7–23 (2003). doi:10.1023/A:1022314423998
14. Land, E.H., McCANN, J.J.: Lightness and Retinex theory. J. Opt. Soc. Am. **61**(1), 1–11 (1971). doi:10.1364/JOSA.61.000001. http://www.opticsinfobase.org/abstract.cfm?URI=josa-61-1-1
15. Logvinenko, A.D.: Lightness induction revisited. PERCEPTION-LONDON-**28**, 803–816 (1999). doi:10.1068/p2801
16. Lysaker, M., Lundervold, A., Tai, X.C.: Noise removal using fourth-order partial differential equation with applications to medical magnetic resonance images in space and time. IEEE Trans Image Process **12**(12), 1579–1590 (2003). doi:10.1109/TIP.2003.819229
17. Lysaker, M., Tai, X.C.: Iterative image restoration combining total variation minimization and a second-order functional. Int. J. Comput. Vis. **66**(1), 5–18 (2006). doi:10.1007/s11263-005-3219-7
18. Ma, W., Morel, J.M., Osher, S., Chien, A.: An ℓ_1-based variational model for retinex theory and its application to medical images. In: CVPR, pp. 153–160. IEEE (2011). doi:10.1137/100806588
19. Ma, W., Osher, S.: A TV bregman iterative model of Retinex theory. Inverse Probl. Imaging **6**(4), 697–708 (2012). doi:10.3934/ipi.2012.6.697
20. Marini, D., Rizzi, A.: A computational approach to color adaptation effects. Image Vis. Comput. **18**(13), 1005–1014 (2000). doi:10.1016/s0262-8856(00)00037
21. Morel, J., Petro, A., Sbert, C.: A PDE formalization of Retinex theory. IEEE Trans. Image Process. **19**(11), 2825–2837 (2010). doi:10.1109/TIP.2010.2049239
22. Ng, M.K., Wang, W.: A total variation model for Retinex. SIAM J. Imaging Sci. **4**(1), 345–365 (2011). doi:10.1137/100806588
23. Papafitsoros, K., Schönlieb, C.: A combined first and second order variational approach for image reconstruction. J. Math. Imaging Vis. **48**(2), 308–338 (2014). doi:10.1007/s10851-013-0445-4
24. Rudin, L.I., Osher, S., Fatemi, E.: Nonlinear total variation based noise removal algorithms. Phys. D **60**(1), 259–268 (1992). doi:10.1016/0167-2789(92)90242-f
25. Setzer, S., Steidl, G.: Variational methods with higher order derivatives in image processing. In: N. Press (ed.) Approximation XII, pp. 360–386. Brentwood (2008)
26. Setzer, S., Steidl, G., Teuber, T.: Infimal convolution regularizations with discrete ℓ_1-type functionals. Comm. Math. Sci. **9**(3), 797–872 (2011). doi:10.4310/cms.2011.v9.n3.a7
27. Tai, X.C., Hahn, J., Chung, G.J.: A fast algorithm for Euler's elastica model using augmented Lagrangian method. SIAM J. Imaging Sci. **4**(1), 313–344 (2011). doi:10.1137/100803730
28. Yin, W., Goldfarb, D., Osher, S.: The total variation regularized L^1 model for multiscale decomposition. Multiscale Model. Simul. **6** (2007). doi:10.1137/060663027
29. Zhang, X., Burger, M., Osher, S.: A unified primal-dual algorithm framework based on Bregman iteration. J. Sci. Comput. **46**(1), 20–46 (2011). doi:10.1137/09076934X
30. Zosso, D., Tran, G., Osher, S.: A unifying retinex model based on non-local differential operators. In: IS&T/SPIE Electronic Imaging, pp. 865,702–865,702. International Society for Optics and Photonics (2013). doi:10.1117/12.2008839

Jingwei Liang is now a Ph.D. candidate in Signal and Image processing at GREYC, ENSICAEN and Université de Caen Base Normandie. Before that, he received his master degree in applied mathematics in 2013 from Shanghai Jiao Tong University, China, and bachelor degree in Electronic and Information Engineering from Nanjing University of Posts and Telecommunications. His current research interests mainly focus on convex optimization and image processing.

Xiaoqun Zhang is an associated professor at department of mathematics and institute of natural sciences in Shanghai Jiao Tong University, Shanghai, China. She received her bachelor and master degrees from Wuhan University, China in 2000 and 2003. She obtained her Ph.D. degree in applied mathematics from University of South Brittany, France in 2006. From July 2007 to July 2010, she worked in University of California, Los Angeles as a CAM assistant professor. Her research interests include mathematical image processing, computer vision, inverse problems and optimization.